Macromolecules

Article

pubs.acs.org/Macromolecules

5,10-Dihydroindolo[3,2-*b*]indole-Based Copolymers with Alternating Donor and Acceptor Moieties for Organic Photovoltaics

Zbyslaw R. Owczarczyk,* Wade A. Braunecker, Andres Garcia, Ross Larsen, Alexandre M. Nardes, Nikos Kopidakis, David S. Ginley, and Dana C. Olson

National Center for Photovoltaics, National Renewable Energy Laboratory, 15013 Denver West Parkway, Golden, Colorado 80401, United States

Supporting Information

ABSTRACT: A series of new donor−acceptor π-conjugated copolymers incorporating 5,10-dihydroindolo[3,2-*b*]indole (DINI) as an electron donating unit have been designed, synthesized, and explored in bulk heterojunction solar cells with diketopyrrolopyrrole and thienopyrroledione as the electron accepting units. A significant effect of the size and shape of the pendant alkyl substituents attached to the DINI unit on the optical and electronic properties of the copolymers is described. Our study reveals a good correlation between the theoretical calculations performed on the selected materials and the experimental HOMO, LUMO, absorption spectra, and band gap energies of the corresponding copolymers. The band gaps of the conjugated copolymers can be tailored over 0.4 eV by the electron-withdrawing nature of the different acceptor units to provide better overlap with the solar spectrum, and the energy levels can be tuned ∼0.2 eV depending on the alkyl substituents employed. For the polymers in this study, a nonoptimized power conversion efficiency as high as 3% was observed.

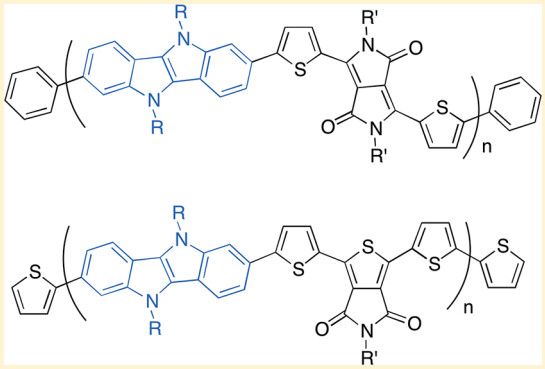

INTRODUCTION

Organic photovoltaic (OPV) devices based on π-delocalized conjugated polymers have attracted considerable interest due to their potential for solution processable, lightweight, flexible, and economically viable solar cells.[1−3] The bulk heterojunction (BHJ) has proven particularly successful for polymer solar cells, wherein the active layer is comprised of an interpenetrating network of a narrow band gap conjugated polymer blended with a fullerene derivative. The morphology of the active layer, particularly phase separation of the polymer/fullerene blend, plays a very important role in determining charge generation and transport properties that are important to the function of the solar cell.[1,4,5] It is critical that a bicontinuous network be formed with large interfacial areas and appropriate domain sizes to facilitate exciton dissociation and transport of separated charges to the corresponding electrodes in the device. Additionally, polymer/fullerene intercalation is also determined by the size and density of the solubilizing alkyl chains along the polymer backbone.[6] Thus, systematic efforts are required to find those alkyl substituents on a polymer absorber that best facilitate the formation of optimal nanoscale phase-separated morphologies.[4−7]

Electronic properties of the organic semiconductors present in the active layer are also critically important to influencing device performance. Ideally, the absorption of the conjugated polymer should have broad overlap with the solar spectrum to maximize photon collection. Additionally, suitable energy levels of the polymer absorber are required to match those of the fullerene acceptors and relatively deep highest occupied molecular orbital (HOMO) of the polymer is desirable to maximize the open circuit voltage (V_{OC}) in OPV devices.[8,9] Conjugated polymers with aromatic backbones comprising alternating units of electron-rich (D) and electron-deficient moieties (A) provide a unique method for fine-tuning polymer band gaps to better harvest an expanded range of the solar spectrum. Additionally, the electron donating/withdrawing strength of the individual components can be adjusted to further fine-tune the HOMO and LUMO values of the polymer to permit efficient photoinduced charge transfer to the fullerene acceptor while maintaining a relatively high V_{OC}, thereby maximizing power conversion efficiency (PCE).[8,9] Consequently, BHJ solar cells containing D−A conjugated copolymer structures exhibit some of the highest PCEs for OPV devices to date.[10,11]

It is well established that polymer absorbers containing a long, planar, π-conjugated backbone can offer broad overlap of their absorption with the solar spectrum and often demonstrate high charge-carrier mobility due to $\pi-\pi$ stacking interactions.[12] However, materials containing unsubstituted multiple fused aromatic rings are notoriously insoluble in common organic solvents used for the fabrication of OPV cells. 5,10-Dihydroindolo[3,2-*b*]indole (DINI) represents a highly π-

Received: September 20, 2012
Revised: January 22, 2013
Published: February 5, 2013

Scheme 1. Synthesis of 5,10-Dihydroindolo[3,2-*b*]indole Comonomers[a]

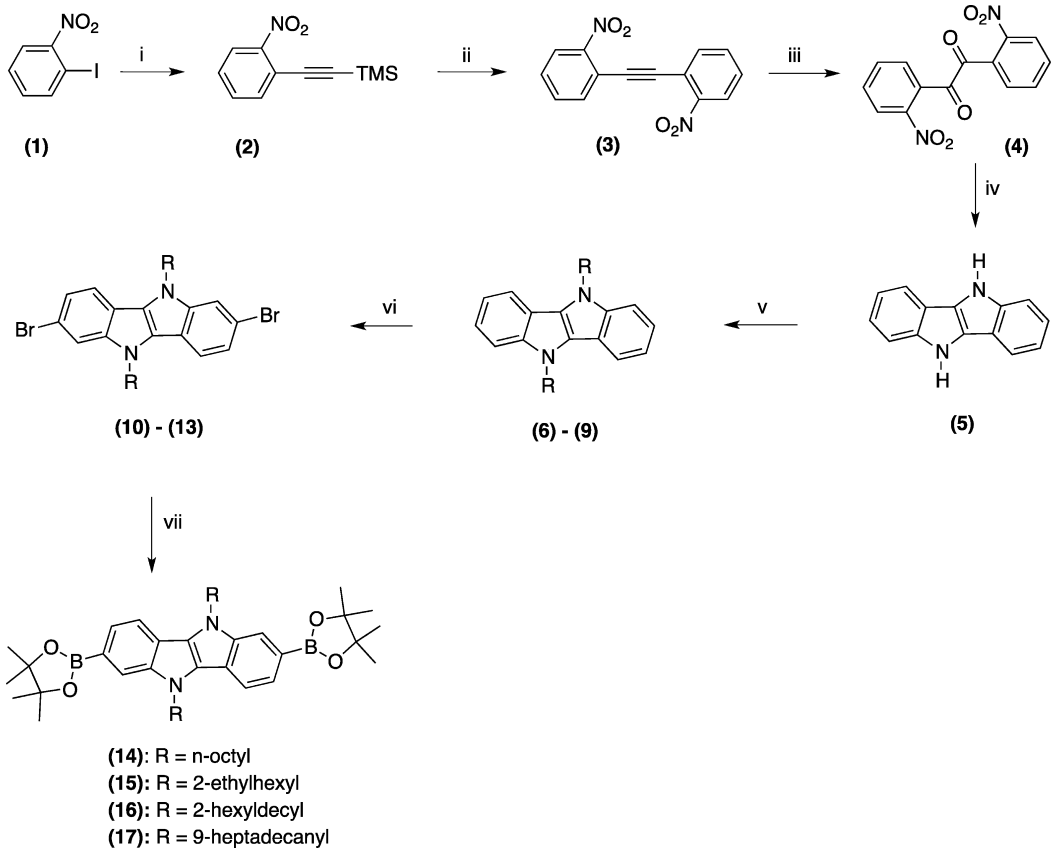

[a]Reagents and conditions: (i) ethynyltrimethylsilane, toluene, Et_3N, cat. $PdCl_2(PPh_3)_2$–CuI, rt, 12 h; (ii) KOH–MeOH, rt, 0.5 h, iodonitrobenzene, toluene, Et_3N, cat. $PdCl_2(PPh_3)_2$–CuI, rt, 12 h; (iii) $KMnO_4$, AcOH, H_2O, cat. TBABr, CH_2Cl_2, refux, 6 h; (iv) Zn, AcOH, HCl, 1 h at 40 °C, then 3 h at 80 °C; (v) alkyl halide or tosylate, NaH, DMF, rt, 8 h; (vi) Br_2, Py/$CHCl_3$, rt, 3 h; (vii) 2.1 equiv of *n*-BuLi, THF, −70 °C, 2 h, then 2-isopropoxy-4,4,5,5-tetramethyl-1,3,2-dioxaborolane, −70 °C to rt, 4 h.

conjugated, electron-rich, and planar aromatic polycyclic fused structure (Scheme 1) that, when copolymerized with an electron-deficient unit (A) in alternating fashion, could lead to strong $\pi-\pi$ interactions among polymer chains and potentially enable broad spectral absorption ideal for OPV applications. The two unsubstituted nitrogen atoms on the opposite sides of the aromatic skeleton of DINI offer a unique opportunity to easily tailor the solubility and alkyl chain density of the polymer. Despite these promising features, to the best of our knowledge, DINI-containing copolymers have never been investigated for OPV applications.

In this work, DINI is copolymerized with the electron accepting moieties diketopyrrolopyrrole (DPP) and thienopyrroledione (TPD). Recently, DPP[13] and TDP[14] based copolymers have emerged as very attractive materials for both thin-film transistors and solar cell devices. The compact planar structure and strong electron-withdrawing ability of DPP and TPD moieties could potentially benefit electron delocalization along copolymer chains via the push–pull effect and promote interchain $\pi-\pi$ stacking. Such interactions should improve charge carrier mobility and significantly affect the self-assembly process, which can be further manipulated by changing the size of alkyl chains on the electron-withdrawing units.[6] Unlike benzothiadiazole, a robust electron withdrawing unit that is widely used in OPV applications, DPP and TPD can be functionalized on the nitrogen atoms with alkyl chains. This not only improves the polymer's solubility but also provides further options for tailoring the alkyl groups along the copolymer backbone. The varied electron withdrawing strengths of DPP and TPD also allow the absolute energy levels of the DINI copolymers to be tuned. Additionally, time-dependent density functional theory computations suggest that D–A copolymers containing DINI with DPP or TPD offer many desirable characteristics that make these polymers attractive candidate materials, including a high extinction coefficient, a broad absorption which overlaps well with the solar spectral spectrum, a relatively low band gap, appropriate energy levels, and a broad delocalization of the HOMO along the polymer backbone. We demonstrate the effect of the side chains on packing in the solid state and correlate stronger coupling of the polymer chains with a further red-shift of the absorption spectrum as well as with improved efficiency for free carrier generation in bulk heterojunctions. Finally, we show that improved free carrier generation leads to higher short-circuit current density in OPV devices under simulated sunlight.

■ EXPERIMENTAL SECTION

Reagents and Instrumentation. All reagents and chemicals were purchased from commercial sources (Aldrich, Acros, Strem, Fluka) and used without further purification unless stated otherwise. All reactions were performed under dry N_2. Solvents were dried when necessary or purified using Mbraun Solvent Purifier. Column chromatography was performed with Fluka Silica Gel 60 (220–400 mesh). All small molecules were characterized by ^{1}H NMR (400 MHz) and ^{13}C NMR (100 MHz) on a Varian Unity Inova. Chemical

dx.doi.org/10.1021/ma301987p | *Macromolecules* 2013, 46, 1350–1360

shifts in the NMR spectra were reported in ppm relative to the singlet at 7.26 ppm for $CDCl_3$. UV−vis absorption measurements were performed using a Hewlett-Packard 8453 UV−vis spectrophotometer. Gel permeation chromatography (GPC) measurements were performed on a PL-Gel 300 × 7.5 mm (5 μm) mixed D column using Agilent 1200 Series GPC-SEC Analysis System.

Polymer Molecular Weight Determination. Polymer samples were dissolved in HPLC grade chloroform (~1 mg/mL), stirred, and heated at 50 °C for several hours, stirred overnight at rt, and then filtered through a 0.45 μm PVDF filter. Size exclusion chromatography was then performed on a PL-Gel 300 × 7.5 mm (5 μm) mixed D column using an Agilent 1200 series autosampler, inline degasser, and refractometer. The column and detector temperatures were 35 °C. HPLC grade chloroform was used as eluent (1 mL/min). Linear polystyrene standards were used for calibration. The same general procedure was performed for larger scale preparatory GPC work. 4.5 mL of a ~3 mg/mL polymer solution in HPLC grade chloroform was injected on two PL-Gel 300 × 25 mm (10 μm) mixed D columns connected in series. An Agilent 1200 series autosampler, inline degasser, and diode array detector were employed. The column and detector temperatures were 25 °C. HPLC grade chloroform was used as eluent (10 mL/min).

Cyclic Voltammetry. All voltammograms were recorded at 25 °C with a CH Instruments Model 600D potentiostat. Measurements were carried out under nitrogen at a scanning rate of 0.1 V s^{-1} using a platinum wire as the working electrode and a platinum wire as the counter electrode. Potentials were measured vs Ag/Ag^+ (and calibrated vs Fc/Fc^+) using 0.01 M $AgClO_4$ and a 0.1 M Bu_4NBF_4 salt bridge to minimize contamination of the analyte with Ag^+ ions. Polymer films were drop-cast onto a platinum wire working electrode from a 1 mg/mL chloroform solution and dried under a stream of nitrogen prior to measurement in a 0.1 M Bu_4NBF_4−acetonitrile solution.

Time-Resolved Microwave Conductivity. TRMC is a pump−probe technique that has been extensively used to measure the photoconductance of a film without the need for charge collection at electrical contacts.[15,16] The details of the experimental methodology have been presented elsewhere.[16,17] In brief, the sample is mounted in a microwave cavity at the end of an X-band waveguide operating at ca. 9 GHz, and is photoexcited through a grid with a laser pulse with a 5 ns laser pulse from an OPO pumped by a Nd:YAG laser. The relative change of the microwave power, P, in the cavity, caused by the photoinduced generation of free electrons and holes, is related to the transient photoconductance, ΔG, by $\Delta P/P = -K\Delta G$, where the calibration factor K is experimentally determined individually for each sample. Taking into account that the electrons and holes are generated in pairs, the photoconductance can be expressed as[16]

$$\Delta G = \beta q_e F_A I_0 (\phi \sum \mu) \quad (1)$$

where q_e is the elementary charge, $\beta = 2.2$ is the geometric factor for the X-band waveguide used, I_0 is the incident photon flux, F_A is the fraction of light absorbed at the excitation wavelength, φ is the quantum efficiency of free carrier generation per photon absiorbed, and $\sum\mu$ is the sum of the mobilities of electrons and holes.[16] Equation 1 allows one to calculate the $\varphi\sum\mu$ product:

$$\phi \sum \mu = \frac{\Delta G}{\beta q_e F_A I_0} \quad (2)$$

At high absorbed photon flux $\varphi\sum\mu$ decreases with I_0 due to higher order processes that limits the charge-carrier generation yield, φ.[16,17] We use eq 3 (below) to fit the light intensity dependence of $\varphi\sum\mu$ and extrapolate to the low intensity range where $\varphi\sum\mu$ does not depend on I_0 (the linear response regime).[16,17]

$$\phi \sum \mu = \frac{A}{1 + \sqrt{BI_0F_A} + CI_0F_A} \quad (3)$$

where A, B, and C are fitting coefficients. At the low intensity range, $\varphi\sum\mu = A$.

Device Fabrication. Pattern glass/ITO substrates (Thin Films Devices, Inc.) for photovoltaic measurements were cleaned prior to device fabrication by sonication in acetone and isopropanol followed by a O_2 plasma treatment at 800 mTorr O_2 pressure and 150 W power for 5 min. Devices with the standard architecture ITO/PEDOT:PSS/BHJ/Ca/Al, where PEDOT:PSS is poly(3,4-ethylenedioxythiophene):poly(styrenesulfonate), were fabricated by spin-coating PEDOT:PSS (Clevios P VP Al 4083) followed by spin-coating of the corresponding polymer:$PC_{61}BM$ solution and completed by thermal deposition of 20 nm of Ca and 100 nm of Al electrodes with an area of 11 mm^2 via a shadow mask at a base pressure of ~3×10^{-8} Torr. The blend ratio of polymer to $PC_{61}BM$ was altered from 1:1 to 1:4.

Polymer BHJ films with ratio 1:2 **P1**−**P8**:$PC_{61}BM$ were deposited from 8 mg/mL polymer concentration in chlorobenzene (CB) or $CHCl_3$ solutions containing various amount (%) by volume 1,8-diiodooctane cosolvent. All BHJ films were fabricated by spin-coating filtered 70 °C solutions with 0.45 μm PTFE filters. Current−voltage measurements of PV devices under a 100 mW/cm^2 illumination intensity (supplied by a tungsten halogen lamp and monitored with Hamamatsu Si photodiodes equipped with KG5 filters) were carried out with a Keithley 236 source-measuring unit in a N_2 atmosphere.

Theoretical Methods. We used a combination of ground-state density functional theory (DFT) and time-dependent density functional theory (TDDFT) to predict the properties of hydrogen-terminated oligomers (with n = 1, 2, 3, 4) for the polymers reported in this work. We performed all calculations using the default settings in the Gaussian 09 electronic structure package, revision B.01,[18] and we optimized the geometry of each oligomer in vacuum using the Becke-style three-parameter density functional with the Lee−Yang−Parr correlation function (B3LYP) with the 6-31G(d) basis set; subsequently, we added diffuse functions to the basis (6-31+G(d)) for calculation of the orbital energies and optical absorption spectra of the optimized structures, as described below. We found that adding diffuse functions had little effect on the predicted absorption spectra; the main change was a systematic shift of the molecular orbital energies down by ~200−300 meV.

To estimate optical absorption spectra, we calculated the lowest 12 excited states with TDDFT. In all cases, the alkyl groups substituents were replaced by methyl groups because we have found that there is a negligible effect on the HOMO and LUMO levels and the absorption spectrum caused by replacing a methyl group with an ethyl or a small branched alkyl group, such as isopropyl. For visualization purposes, we broadened the predicted absorption spectra by convolving the discrete gas-phase spectrum with a Gaussian having full width at half-maximum of 0.15 eV and transforming the resulting spectra from functions of energy to functions of wavelength with the appropriate hc/λ^2 Jacobian factor. The 0.15 eV broadening was determined empirically by comparing the widths of typical spectra reported in the literature for donor−acceptor type copolymers; no attempt was made to tune this broadening to better match the measured spectra. For each oligomer, the energy gap, E_g, is defined as the lowest energy excitation; note that this energy corresponds to the reddest peak maximum in an absorption spectrum rather than the absorption onset which often is reported from experiment. We also report the energy of an electron in the excited state as the optical LUMO (O-LUMO), which is the calculated HOMO value plus the energy gap; physically, the O-LUMO value seems most relevant for predicting whether exciton dissociation may occur by injection of an electron into an electron accepting species.

Images of molecular geometries and molecular orbitals were generated with Jmol, an open-source Java viewer for chemical structures in 3D.[19] We display HOMO and LUMO contour levels encompassing 80% of the total electron density for each orbital.

Synthesis of Comonomers. *1,2-Bis(2-nitrophenyl)ethyne (**3**).* 2-Iodonitrobenzene (24.9 g, 0.10 mol) was dissolved in dry toluene (220 mL) and triethylamine (25 mL), the solution was purged with nitrogen, and $PdCl_2(Ph_3P)_2$ (230 mg, 0.4 mmol) and CuI (115 mg, 0.6 mmol) were added, followed by (trimethylsilyl)acetylene (15.5 mL, 0.11 mol). The mixture was stirred for 12 h, hexane (80 mL) was

added, and the suspension was filtered through a Celite plug. The resulting eluate was concentrated, the oily residue was dissolved in methanol (100 mL), and a solution of KOH (7.0 g) in methanol (60 mL) was slowly added while maintaining the temperature below 25 °C. The mixture was stirred for 0.5 h, concentrated to ca. 100 mL, poured into water (500 mL), and the product was extracted with ethyl acetate. The extract was dried with sodium sulfate and filtered through a short plug of silica prior to evaporation. The resulting crude (**2**) was dissolved in toluene (200 mL) containing triethylamine (25 mL) and 2-iodonitrobenzene (23.0 g), the solution was purged with nitrogen, and $PdCl_2(Ph_3P)_2$ (230 mg, 0.4 mmol) and CuI (115 mg, 0.6 mmol) were added. The mixture was stirred for 12 h at rt, and the resulting yellow precipitate was isolated by filtration and crystallized from toluene to give 13.67 g (51% yield) of light-yellow solid; mp 187−189 °C dec (lit.[20] 188−189 °C). ^{1}H NMR (400 MHz, $CDCl_3$): δ 7.50−7.56 (m, 2H), 7.63−7.69 (m, 2H), 7.83 (d, J = 7.8 Hz, 2H), 8.14 (d, J = 8.3 Hz, 2H). ^{13}C NMR (100 MHz, $CDCl_3$): δ 91.95, 118.07, 124.83, 129.54, 133.11, 135.26, 149.48.

*1,2-Bis(2-nitrophenyl)ethane-1,2-dione (**4**).* Compound **3** (19.94 g, 74 mmol) was added to a mixture of potassium permanganate (35.2 g, 222 mmol), water (600 mL), TBAB (0.48 g, 1 mmol), methylene chloride (800 mL), and acetic acid (40 mL). The mixture was vigorously stirred at reflux for 7 h, cooled, and carefully decolorized with $NaHSO_3$. The organic and aqueous were separated, and the yellow organic was dried with Na_2SO_4 and filtered through Celite plug. After removal of solvent the resulting yellow crystalline solid was washed with methanol to give 18.90 g (85% yield) of the title compound; mp 206−207 °C (lit.[21] 205−206 °C). ^{1}H NMR (400 MHz, $CDCl_3$): δ 7.70 (dd, J_1 = 7.6 Hz, J_2 = 1.2 Hz, 2H), 7.73−7.79 (m, 2H), 7.86−7.91 (m, 2H), 8.29 (dd, J_1 = 8.3 Hz, J_2 = 0.5 Hz, 2H).

*5,10-Dihydroindolo[3,2-b]indole[27] (**5**).* To a stirred mixture containing acetic acid (360 mL) and Zn powder (45.8 g, 700 mmol) was added 12 N HCl (3 mL) followed by **4** (21.00 g, 70 mmol), which was added in portions over 0.5 h while maintaining temperature below 40 °C. The mixture was stirred at 80 °C for 1 h, an additional amount of Zn (9.81 g, 200 mmol) was added, and stirring was continued for another 2 h, before the reaction mixture was cooled to rt. The solids containing unreacted Zn and the product were isolated by filtration and washed twice with methanol, and the product was eluted with hot DMF (70−80 °C, 3 × 50 mL). The cold eluent was poured slowly to stirred cold water (1200 mL), precipitated white solid was isolated by filtration, washed with water, several times with methanol, and dried initially in air and then under vacuum to yield 13.06 g (91%) of the title compound. ^{1}H NMR (400 MHz, acetone-d_6): δ 7.53 (d, J = 8.1 Hz, 2 H), 7.78 (d, J = 7.8 Hz, 2H), 7.53 (d, J = 8.1 Hz, 2 H), 7.16−7.20 (m, 2 H), 7.06−7.10 (m, 2 H).

*5,10-Di(n-octyl)-5,10-dihydroindolo[3,2-b]indole (**6**). General Procedure.* This compound was synthesized according to modified literature procedure.[22] NaH (2.64 g, 55 mmol, 50% in mineral oil) was stirred with hexane (25 mL) under nitrogen for a few minutes before stirring was turned off to allow NaH to settle at the bottom of the flask. After 30 min, the hexane solution was removed under a slight nitrogen pressure, using cannula tipped with a soft filter paper. The activated NaH was mixed with dry DMF (45 mL). Subsequently, **5** (4.08 g, 20 mmol) was added to the mixture in portions, followed by *n*-octyl bromide (7.8 mL, 45 mmol), while maintaining temperature of the reaction mixture below 35 °C. The mixture was then stirred for 10 h at rt before it was poured slowly into cold water (600 mL). The precipitated solid material was isolated by filtration, washed with water and methanol, and dried under vacuum to yield 8.10 g (94%). ^{1}H NMR (400 MHz, $CDCl_3$): δ 7.82 (d, 2H, J = 7.8 Hz), 7.44 (d, 2H, J = 8.1 Hz), 7.30 (t, 2H), 7.16 (t, 2H), 4.35 (t, 4H, J = 7.2 Hz), 1.91 (m, 4H), 1.18−1.44 (m, 20H), 0.86 (t, 6H, J = 7.2 Hz). ^{13}C NMR (100 MHz, $CDCl_3$): δ 140.95, 126.17, 121.32, 117.78, 114.56, 109.91, 49.56, 45.40, 31.74, 31.12, 29.26, 29.02, 27.00, 22.53, 14.02.

*5,10-Bis(2-ethylhexyl)-5,10-dihydroindolo[3,2-b]indole (**7**).* Yield: 96%. ^{1}H NMR (400 MHz, $CDCl_3$): δ 7.84 (d, 2H, J = 7.8 Hz), 7.45 (d, 2H, J = 8.2 Hz), 7.29 (t, 2H), 7.17 (t, 2H), 4.36 (m, 4H), 2.19 (m, 2H), 1.20−1.45(m, 16H), 0.92 (t, 6H, J = 7.2 Hz), 0.85 (t, 6H, J = 7.2 Hz). ^{13}C NMR (100 MHz, $CDCl_3$): δ 140.92, 126.21, 121.34, 117.78, 114.52, 109.90, 49.57, 40.34, 30.86, 28.75, 24.23, 23.04, 13.98, 10.92.

*5,10-Bis(2-hexyldecyl)-5,10-dihydroindolo[3,2-b]indole (**8**).* This compound was synthesized according to the general procedure described above using 2-hexyldecyl *p*-toluenesulfonate[23] in place of an alkyl halide. Compound **8** was isolated in 84% yield as a pale yellow solid. ^{1}H NMR (400 MHz, $CDCl_3$): δ 7.81 (d, 2H, J = 8.0 Hz), 7.42 (d, 2H, J = 8.4 Hz), 7.26 (t, 2H), 7.14 (t, 2H), 4.43 (d, 4H, J = 7.4 Hz), 2.23 (m, 2H), 1.17−1.36 (m, 48H), 0.84 (m, 12H). ^{13}C NMR (100 MHz, $CDCl_3$): δ 140.98, 126.17, 121.31, 117.76, 114.57, 109.91, 49.94, 38.87, 31.85, 31.77, 29.95, 29.63, 29.49, 29.24, 26.53, 26.50, 22.65, 22.58, 14.10, 14.05.

*5,10-Di(heptadecan-9-yl)-5,10-dihydroindolo[3,2-b]indole (**9**).* This compound was synthesized according to a general procedure using 9-heptadecane *p*-toluenesulfonate in 90% yield. ^{1}H NMR (400 MHz, $CDCl_3$): δ 7.92 (d, 2H, J = 7.8 Hz), 7.42−7.68 (m, 2H), 7.08−7.33 (m, 4H), 4.50−4.95 (m, 2H), 2.32 (m, 4H), 2.00 (m, 4H), 0.94−1.30 (m, 48H), 0.81 (t, 12H, J = 7.2 Hz). Multiples and broad protons are due to a phenomenon of atropisomerism. ^{13}C NMR (100 MHz, $CDCl_3$): δ 142.03. 125.06, 121.25, 119.84, 117.58, 113.77, 112.64, 109.87, 59.98, 56.02, 35.14, 34.41, 31.74, 29.34, 29.31, 29.13, 26.94, 22.56, 14.04 (multiple carbon peaks are due to the phenomenon of atropisomerism).[24]

*2,7-Dibromo-5,10-bis(n-octyl)-5,10-dihydroindolo[3,2-b]indole (**10**). General Procedure.* This compound was synthesized according to a modified literature procedure.[22] To a solution of the crude **6** (4.30 g, 10 mmol) in a mixture of pyridine (8 mL) and chloroform (10 mL) was added Br_2 (1.1 mL, 21.5 mmol) in chloroform (10 mL) over a period of 30 min. After 2 h, the mixture was poured into 1 N HCl (200 mL) and ice, the product was extracted twice with ethyl acetate, and the combined organic layers were washed twice with water and dried over Na_2SO_4 prior to evaporation. The crude product was crystallized from methanol−ethyl acetate to yield 3.59 g (61%) of the title compound as a yellow solid. ^{1}H NMR (400 MHz, $CDCl_3$): δ 7.62 (d, 2H, J = 8.4 Hz), 7.56 (d, 2H, J = 1.6 Hz), 7.26 (dd, 2H, J_1 = 8.4 Hz, J_2 = 1.6 Hz), 4.34 (t, 4H, J = 7.2 Hz), 1.90 (m, 4H), 1.17−1.41 (m, 20H), 0.85 (t, 6H, J = 7.0 Hz). ^{13}C NMR (100 MHz, $CDCl_3$): δ 141.09, 125.77, 121.37, 118.60, 115.34, 113.11, 112.73, 45.41, 31.74, 31.10, 29.28, 29.09, 27.03, 22.56, 14.03.

*2,7-Dibromo-5,10-bis(2-ethylhexyl)-5,10-dihydroindolo[3,2-b]-indole (**11**).* Yield 61%; a light orange solid. ^{1}H NMR (400 MHz, $CDCl_3$): δ 7.60 (d, 2H, J = 8.5 Hz), 7.52 (d, 2H, J = 1.5 Hz), 7.24 (dd, 2H, J_1 = 8.5 Hz, J_2 = 1.5 Hz), 4.18 (m, 4H), 2.06 (m, 2H), 1.16−1.42 (m, 16H), 0.88 (t, 6H, J = 7.4 Hz), 0.81 (t, 6H, J = 7.2 Hz). ^{13}C NMR (100 MHz, $CDCl_3$): δ 141.39, 125.86, 121.15, 118.66, 115.18, 112.96, 112.83, 49.72, 38.53, 31.84, 31.72, 31.58, 31.60, 29.87, 29.56, 29.44, 29.24, 26.39, 22.64, 22.58, 14.10, 14.04.

*2,7-Dibromo-5,10-bis(2-hexyldecyl)-5,10-dihydroindolo[3,2-b]-indole (**12**).* This compound was synthesized according to a general procedure, except that after work-up, the crude material was extracted from aqueous mixture with ethyl acetate, the organic layer was dried over sodium sulfate prior to evaporation of the solvent, and the crude product was purified on a short silica gel plug using hexane as an eluent to give a light orange oil in 80% yield. ^{1}H NMR (400 MHz, $CDCl_3$): δ 7.60 (d, 2H, J = 8.4 Hz), 7.52 (d, 2H, J = 1.2 Hz), 7.23 (dd, 2H, J_1 = 8.4 Hz, J_2 = 1.2 Hz), 4.20 (d, 4H, J = 7.0 Hz), 2.12 (m, 2H), 1.16−1.40 (m, 48H), 0.86 (m, 12H). ^{13}C NMR (100 MHz, $CDCl_3$): δ 141.18, 125.80, 121.21, 118.62, 115.19, 112.98, 112.79, 50.21, 39.01, 31.93, 31.80, 30.01, 29.80, 29.29, 26.60, 26.42, 22.70, 22.65, 14.20, 14.09.

*2,7-Dibromo-5,10-bis(heptadecan-9-yl)-5,10-dihydroindolo[3,2-b]indole (**13**).* Yield 81%; a light orange solid. ^{1}H NMR (400 MHz, $CDCl_3$): δ 7.72 (d, 2H, J = 8.2 Hz), 7.62 (bs, 2H), 7.26 (bs, 2H), 4.27−4.83 (m, 2H), 2.22 (m, 4H), 1.87 (m, 4H), 0.90−1.28 (m, 48H), 0.80 (t, 12H, J = 7.2 Hz) (multiple and broad protons are due to a phenomenon of atropisomerism).[24]

^{13}C NMR (100 MHz, $CDCl_3$): δ 142.74, 125.02, 121.16, 120.83, 115.41, 112.94, 112.41, 56.55, 34.95, 31.73, 29.24, 29.07, 26.76, 22.56, 14.04 (multiple carbon peaks are due to the phenomenon of atropisomerism).[24]

*5,10-Bis(n-octyl)-2,7-bis(4,4,5,5-tetramethyl-1,3,2-dioxaborolan-2-yl)-5,10-dihydroindolo[3,2-b]indole (**14**). General Procedure.* This compound was synthesized according to modified literature procedure.[25] To a solution of compound **10** (2.35 g, 4.0 mmol) in THF (40 mL) was added dropwise 3.60 mL (9.0 mmol) of *n*-butyllithium (2.5 M in hexane) at −70 °C. The mixture was stirred at −78 °C for 2 h, and 2-isopropoxy-4,4,5,5-tetramethyl-1,3,2-dioxaborolane (2.65 mL, 13,0 mmol) was added rapidly to the suspension of the bis-lithium salt in THF. After an additional 1 h at −78 °C, the resulting mixture was warmed up to rt and stirred for 6 h, before it was poured into cold water (300 mL), extracted with ethyl acetate, and dried over sodium sulfate. The solvent was removed under reduced pressure, and the residue was purified by crystallization form methanol/ethyl acetate to yield the title product as light yellow crystals (1.73 g, 63%). ^{1}H NMR (400 MHz, $CDCl_3$): δ 7.95 (s, 2H), 7.84 (d, 2H, J = 7.8 Hz), 7.62 (d, 2H, J = 7.9 Hz), 4.54 (t, 4H, J = 7.2 Hz), 1.98 (m, 2H), 1.40 (s, 24H), 1.14−1.50 (m, 20H). ^{13}C NMR (100 MHz, $CDCl_3$): δ 140.48, 127.17, 124.03, 121.80, 117.21, 116.36, 116.24, 83.58, 45.18, 31.80. 30.38, 29.39, 29.14, 22.58, 14.06.

*5,10-Bis(2-ethylhexyl)-2,7-bis(4,4,5,5-tetramethyl-1,3,2-dioxaborolan-2-yl)-5,10-dihydroindolo[3,2-b]indole (**15**).* Yield: 57%; light yellow crystals (1.57 g, 57%). ^{1}H NMR (400 MHz, $CDCl_3$): δ 7.93 (bs, 2H), 7.83 (d, 2H, J = 7.8 Hz), 7.61 (d, 2H, J = 7.8 Hz), 4.41 (m, 4H), 2.19 (m, 2H), 1.39 (bs, 24H), 1.19−1.44 (m, 16H), 0.87 (m, 12H). ^{13}C NMR (100 MHz, $CDCl_3$): δ 141.02, 127.36, 123.86, 121.48, 117.35, 116.67, 116.18, 83.53, 49.35. 40.28, 30.66, 28.65, 24.94, 24.89, 24.25, 23.00, 14.04, 10.98.

*5,10-Bis(2-hexyldecyl)-2,7-bis(4,4,5,5-tetramethyl-1,3,2-dioxaborolan-2-yl)-5,10-dihydroindolo[3,2-b]indole (**16**).* This material was synthesized according to the general procedure in 42% yield as an oil, after purification on silica gel using a mixture of ethyl acetate and hexane (1:7) as an eluent (R_f 0.25). ^{1}H NMR (400 MHz, $CDCl_3$): δ 7.92 (s, 2H), 7.82 (d, 2H, J = 8.0 Hz), 7.59 (d, 2H, J = 8.0 Hz), 4.40 (d, 4H, J = 7.4 Hz), 2.25 (m, 2H), 1.17−1.38 (m, 48H), 0.84 (m, 12H). ^{13}C NMR (100 MHz, $CDCl_3$): δ 141.04, 127.35, 123.88, 117.31, 116.67, 116.22, 83.46, 49.58, 38.74, 31.85, 31.76, 31.57, 29.89, 29.59, 29.49, 29.24, 26.48, 26.42, 24.88, 22.64, 22.55, 14.09, 14.05.

*5,10-Di(heptadecan-9-yl)-2,7-bis(4,4,5,5-tetramethyl-1,3,2-dioxaborolan-2-yl)-5,10-dihydroindolo[3,2-b]indole (**17**).* Yield 68%; a white solid. ^{1}H NMR (400 MHz, $CDCl_3$): δ 8.02 (s, 2H), 7.95 (d, 2H, J = 8.0 Hz), 7.64 (d, 2H, J = 8.0 Hz), 4.63−5.00 (m, 2H), 2.33 (m, 4H), 2.03 (m, 4H), 1.41 (s, 24H), 0.97−1.34 (m, 48H), 0.82 (t, 12H, J = 7.0 Hz). ^{13}C NMR (100 MHz, $CDCl_3$): δ 142.03, 126.31, 123.71, 121.31, 119.37, 116, 70, 115.35, 83.47, 55.84, 35.07, 31.73, 29.45, 29. 32, 29.26, 29.13, 26.67, 24.86, 24.52, 22.54, 14.02 (multiple carbon peaks are due to the phenomenon of atropisomerism).[24]

*1,3-Bis(5-(trimethylstannyl)thiophen-2-yl)-5-(2-ethylhexyl)-thieno[3,4-c]pyrrole-4,6-dione (**18**).* The brominated precursor of **18**, 1,3-bis(5-bromothiophen-2-yl)-5-(2-ethylhexyl)thieno[3,4-*c*]pyrrole-4,6-dione, was synthesized according to a literature procedure.[26] Compound **18** was synthesized in the following manner according to a modified literature procedure.[27] The precursor (1.00 g, 1.70 mmol) was dissolved in 20 mL of dry THF and cooled to −78 °C under N_2. A *n*-butyllithium solution (2.5 M, 1.50 mL, 3.75 mmol) was added dropwise, and the reaction mixture was stirred for 1 h at −78 °C. Trimethyltin chloride solution (1 M, 4.3 mL, 4.30 mmol) was added dropwise at −78 °C; the reaction was warmed to rt and stirred overnight. The mixture was quenched with 50 mL of water and extracted twice with 100 mL of ethyl acetate. The combined organic phase was dried over $MgSO_4$, and solvent was evaporated. The residue was precipitated from isopropanol to yield 0.38 g (30%) of the title compound as an orange solid. ^{1}H NMR (400 MHz, $CDCl_3$): δ 8.06 (s, 2H), 7.16 (s, 2H), 3.54 (d, 2H), 1.84 (m, 1H), 1.40−1.20 (m, 8H), 0.95 (m, 6H), 0.44 (s, 18H). ^{13}C NMR (100 MHz, $CDCl_3$): δ 163.72, 144.29, 138.54, 137.11, 136.95, 131.36, 128.30, 43.17, 38.85, 31.25, 29.26, 24.55, 23.71, 14.73, 11.13, −7.49.

*Typical Proceedure for Polymer Synthesis. Poly[[5,10-bis(alkyl)-5,10-dihydroindolo[3,2-b]indole-2,7-diyl-alt-[2,5-bis(2-ethylhexyl)-2,3,5,6-tetrahydro-3,6-dioxopyrrolo[3,4-c]pyrrole-1,4-diyl]] (**P2**−**P5**).* DPP comonomer (0.20 mmol), DINI comonomer (0.21 mmol), $Pd_2(dba)_3$−$CHCl_3$ complex (1.5% mol, 3.0 mg), SPHOS (9% mol, 8.0 mg), and dibenzo-18-crown-6 (5% mol, 3.6 mg) were dissolved in 10 mL of toluene, followed by addition of 1.0 mL of K_3PO_4 (2.5 M). The mixture was purged with nitrogen for 10 min and then vigorously stirred at 105 °C for 60 h, before bromobenzene (6 μL, 0.045 mmol) was injected to the reaction mixture. Three hours later, phenylboronic acid (8.5 mg, 0.06 mmol) was added, and the reaction mixture was stirred for an additional 5 h to complete the end-capping process. A palladium scavenger complexing ligand (*N*,*N*-diethylphenylazothioformamide)[28] was then stirred with the reaction mixture for 30 min before the polymer was precipitated into 200 mL of MeOH−H_2O (15−1) mixture, filtered off, washed with methanol, water, and acetone, and subsequently was purified via Soxhlet extraction with acetone and chloroform. The chloroform fraction was concentrated under reduced pressure, the material was reprecipitated into methanol (150 mL), isolated by filtration, washed with methanol, and vacuum-dried overnight to yield the corresponding polymer in 50−80% yield.

*Copolymers **6**−**8**.* Comonomer **18** (88.0 mg, 0.21 mmol), DINI comonomer (0.21 mmol), $Pd_2(dba)_3$−$CHCl_3$ complex (2 mol %), and tri(*o*-tolyl)phosphine (8 mol %) were placed in a flask, purged with three nitrogen/vacuum cycles, and subsequently dissolved in 5 mL of dry chlorobenzene, from which oxygen was removed by purging with nitrogen for 1 h. The mixture was stirred for 36 h at 110 °C, after which 20 μL of 2-bromothiophene was injected as a capping agent. The reaction was stirred for 2 h at 110 °C before 20 μL of 2-(tributyltin)thiophene was injected to complete the end-capping. After an additional 2 h of stirring, a complexing ligand (*N*,*N*-diethylphenylazothioformamide)[28] was stirred with the polymer to remove any residual catalyst before being cooled to rt and precipitated into methanol (100 mL). The precipitate was purified via Soxhlet extraction overnight with methanol, for 2 h with acetone, and finally was collected with chloroform. The chloroform solution was then concentrated by evaporation; the material was reprecipitated into methanol (150 mL), isolated by filtration, washed with methanol, and vacuum-dried overnight to yield the corresponding polymer in 55−75% yield.

*Copolymer **P2**.* ^{1}H NMR (400 MHz, $CDCl_3$): δ 9.0−9.2 (m, 2H), 7.0−7.8 (m, 8H), 3.7−4.5 (m, 8H), 0.6−2.3 (m, 60H).

*Copolymer **P3**.* ^{1}H NMR (400 MHz, $CDCl_3$): δ 7.5−8.0 (m, 10H), 4.2−4.5 (m, 8H), 2.1−2.3 (m, 4H), 1.0−1.4 (m, 48H), 0.7−0.9 (m, 24H).

*Copolymer **P4**.* ^{1}H NMR (400 MHz, $CDCl_3$): δ 9.1 (bs, 2H), 7.4−8.0 (m, 8H), 4.1−4.9 (m, 6H), 1.9−2.4 (m, 10H), 0.7−1.6 (m, 96H).

*Copolymer **P5**.* ^{1}H NMR (400 MHz, $CDCl_3$): δ 9.1 (bs, 2H), 7.4−8.0 (m, 8H), 4.2−4.9 (m, 6H), 1.8−2.5 (m, 12H), 0.7−0.9 (m, 18H), 1.0−1.6 (m, 68H).

*Copolymer **P7**.* ^{1}H NMR (400 MHz, $CDCl_3$): δ 6.7−8.4 (m, H10), 4.2−4.5 (m, 4H), 3.5−3.7 (m, 2H), 1.8−2.1(m, 3H), 0.5−1.7(m, 74H).

*Copolymer **P8**.* ^{1}H NMR (400 MHz, $CDCl_3$): δ 7.2−8.2 (m, 10H), 4.4−4.9 (m, 2H), 3.4−3.6 (m, 2H), 1.7−2.5 (m, 9H), 0.6−1.6 (m, 74H).

RESULTS AND DISCUSSION

Material Synthesis. The synthesis of DINI, as described in the Experimental Section, was prepared using modified literature procedure[29] and is illustrated in Scheme 1. Following the Sonogashira Pd-catalyzed cross-coupling of *o*-iodonitrobenzene (**1**) with ethynyltrimethylsilane to yield trimethyl((2-nitrophenyl)ethynyl)silane (**2**), which was treated with KOH to remove trimethylsilyl group, the resulting acetylene intermediate was reacted with another equivalent of **1** to yield 1,2-bis(2-nitrophenyl)ethyne (**3**). After the oxidation of **3** to the dione **4**, ring closure was accomplished by reductive condensation to give 5,10-dihydroindolo[3,2-*b*]indole (**5**). Subsequent alkylation reactions were performed in DMF using a moderate excess of NaH. Derivatives of 3,6-bis(5-bromo-thiophen-2-yl)-2,5-dialkylpyrrolo[3,4-*c*]pyrrole-1,4-dione (DPP) were prepared

Scheme 2. Synthesis of DPP−5,10-Dihydroindolo[3,2-*b*]indole Copolymers[a]

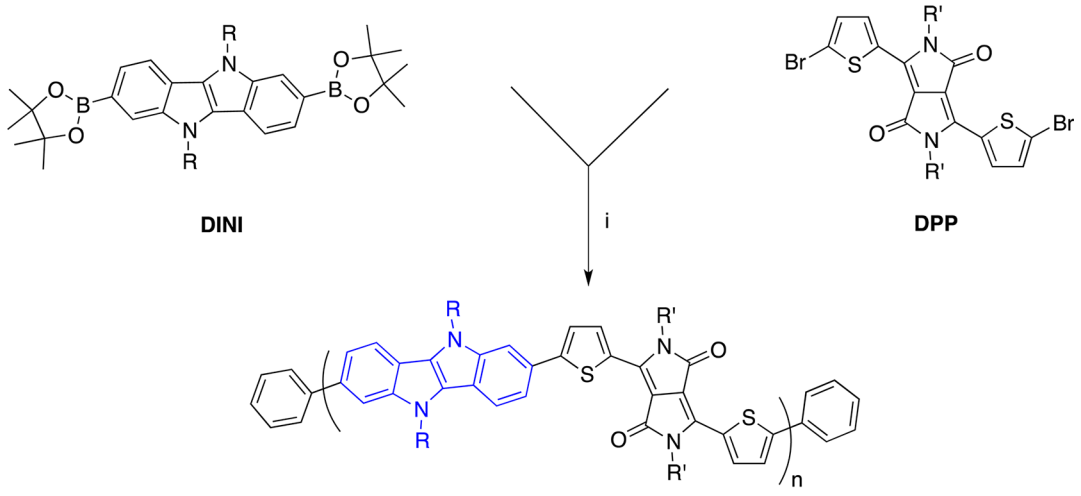

[a]Reagents and conditions: (i) cat. $Pd_2(dba)_3$-*o*-Tol_3P or SPHOS, K_3PO_4(aq), toluene, 105 °C, 60 h, then end-capping with phenylboronic acid and bromobenzene.

according to previously reported procedure.[13] The stannylated derivative of thienopyrroledione (TPD) depicted in Scheme 2 was synthesized from its brominated precursor.[27] As depicted in Scheme 2, copolymers of DPP and DINI (**P1**−**P5**) were synthesized via a Suzuki Pd-catalyzed cross-coupling polymerization protocol in toluene at 105 °C using an aqueous solution of K_3PO_4 as the hydroxyl anion source. During the course of our study, it was found that a more basic aqueous solution of K_3PO_4 was superior to K_2CO_3 in that it produced the desired copolymer in higher yield.[30] End-capping of the polymers was performed using phenylboronic acid and 2-bromobenzene to terminate residual active functionalities, which has been shown to improve performance in photovoltaic devices.[31] A palladium scavenger was added to the reaction and stirred for 30 min prior to work-up to facilitate catalyst removal before polymer precipitation into methanol. The crude material was then purified via Soxhlet extraction with MeOH followed by acetone to remove oligomeric materials.

As bulky branched substituents on the polymer can have a negative effect on carrier mobility if $\pi-\pi$ stacking between the polymer chains is disrupted,[32] we first attempted to synthesize a DPP−DINI copolymer using as little alkyl chain density as possible. **P1** was synthesized with a linear *n*-octyl substituent on the DINI unit and 2-ethylhexyl on DPP. However, **P1** proved quite insoluble in common organic solvents such as chloroform, toluene, chlorobenzene, and DMF, even at temperatures above 100 °C. The introduction of a branched 2-ethylhexyl alkyl group onto DINI resulted in noticeable improvement in solubility of **P2** in common organic solvents; however, the highest number-average molecular weight (M_n) that could be attained for **P2** under these conditions was only 5.2 kg mol^{-1}. We thus resorted to much larger branched alkyl derivatives. When primary 2-hexyldecyl and secondary 9-heptadecanyl alkyl substituents were employed on DINI to synthesize copolymers **P3**−**P5**, solubility was dramatically improved and M_n approaching 50 kg mol^{-1} was achieved (Table 1).

Table 1. Number-Average Molecular Weight (M_n), Polydispersity Index (PDI), and Optical and Electrochemical Properties of Polymers

polymer	M_n (kDa)	PDI	$\lambda_{max}/\lambda_{0.1max}$[b] (nm)	E_g^{opt}[d] (eV)	E_{HOMO}[e] (eV)
P2	5.20	1.7	744/805	1.54	−5.0
P3	15.1	1.9	752/800	1.55	−5.1
P4	20.3	3.0	696/752	1.65	−5.2
P5	49.0	2.6	692/753	1.65	−5.2
P6	–[a]	–	530/625[c]	1.99	−5.1
P7	10.0	1.4	532/630	1.97	−5.2
P8	15.2	1.4	520/607	2.04	−5.3

[a]Not sufficiently soluble for SEC measurements at RT. [b]Measured in chloroform solution; $\lambda_{0.1max}$ = wavelength at which absorption is 0.1 its maximum value. [c]Measured in dichlorobenzene solution. [d]Calculated from solution $\lambda_{0.1max}$. [e]E_{HOMO} estimated from $E_{1/2}$ measured vs Ag/Ag$^+$ in acetonitrile and calibrated against Fc/Fc$^+$ (measured as 0.09 V vs Ag/Ag$^+$); $E_{1/2} = (E_{p,a} + E_{p,c})/2$, where $E_{p,a}$ and $E_{p,c}$ are the peak potentials of the oxidation and reduction waves, respectively; Fc/Fc$^+$ energy level used in HOMO calculations was −4.80 eV.[34]

While our theoretical calculations (*vide infra*) indicated that these D−A copolymers containing DPP and DINI should have quite low energy gaps, they also predicted that the HOMO values would not be very deep. Thus, D−A copolymers of the electron withdrawing TPD were also synthesized with DINI, as copolymers of TPD are known for their relatively deep HOMO values and consequently large values of V_{OC} in OPV devices.[33] Copolymers containing TPD in BHJ solar cells have also recently delivered PCE in excess of 6%.[33] Unfortunately, we were not successful in synthesizing TPD and DINI copolymers under the basic conditions required for Suzuki coupling, as the

dx.doi.org/10.1021/ma301987p | *Macromolecules* 2013, 46, 1350−1360

Scheme 3. Synthesis of TPD−5,10-Dihydroindolo[3,2-*b*]indole Copolymers[a]

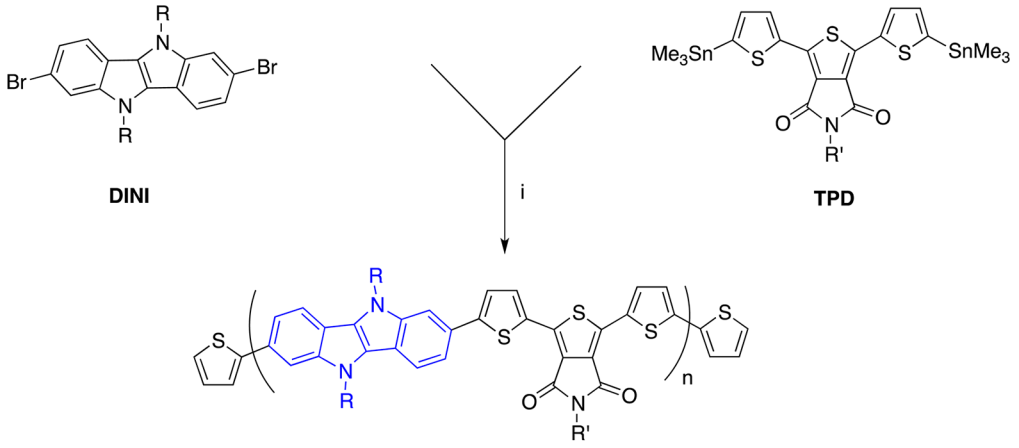

[a]Reagents and conditions: (i) cat. $Pd_2(dba)_3$/*o*-Tol_3P, chlorobenzene, 105 °C, 60 h, then end-capping with 2-(tributylstannyl)thiophene and 2-bromothiophene.

imide functionality in the TPD unit is base sensitive. All attempts to directly stannylate the TPD unit for a Stille coupling polymerization failed; however, we were successful in stannylating the 1,3-bis(thiophenyl)-TPD compound in Scheme 3. Thus, copolymers containing TPD and DINI were synthesized by a Pd-catalyzed Stille cross-coupling copolymerization at 110 °C over 36 h in chlorobenzene, followed by similar end-capping and purification procedures described above. **P6**, having 2-ethylhexyl groups on both the TPD and DINI units, was not sufficiently soluble for molecular weight measurement at room temperature on our GPC. However, the introduction of 2-hexyldecyl and 9-heptadecanyl groups onto DINI gave the soluble polymers **P7** and **P8**. Note that the stannylated TPD compound does not appear to be particularly stable at high temperatures; thus, values of M_n higher than about 8 kg mol^{-1} for **P7** and **P8** could not be directly achieved. The values of 10 and 15 kg mol^{-1} reported in Table 1 were acquired only after purification of the polymer samples with a preparatory GPC.

Theoretical Calculations. HOMO and LUMO energy levels were calculated for oligomers n = 1−4 (where n = 1 is a D−A pair), together with absorption spectra, for copolymers based on DPP−DINI and TPD−DINI. Most of our discussion will be confined to the n = 4 case, which is approaching the polymer limit as evidenced by the convergence of the values in Table 2. As shown in Table 2, the HOMO values for the TPD containing oligomer are predicted to be 190 meV deeper than that containing DPP. Meanwhile, the energy gap for the DPP oligomer is predicted to be 310 meV more narrow than that of TPD. Although some small discrepancies between computed and measured values are observed, both of these results are qualitatively in good agreement with measured values (see Figure 1 and compare Tables 1 and 2).

The geometric structures of DPP−DINI and TPD−DINI tetramers are illustrated in Figure S1 of the Supporting Information. As seen in this figure, all oligomers are quite planar, with dihedral angles between the alternating units being less than 5°. Such planarity should facilitate $\pi-\pi$ stacking interactions. However, the different alkyl substituents can in principle dramatically affect such interactions, which in turn can influence absorption and the efficiency of free carrier generation in the copolymer/fullerene blend. As illustrated at the top of Figure 2, when branching occurs at the 1-position of the secondary alkyl substituent (as is the case for the 9-heptadecanyl substituents in **P4**, **P5**, and **P8**), steric interactions will twist the side chains out of planarity with the polymer backbone, effectively reducing interchain interactions between otherwise planar backbone structures. On the other hand, when the branching occurs in the 2-position (as in the 2-hexyldecyl and 2-ethylhexyl substituents in **P2**, **P3**, **P6**, and **P7**), the alkyl substituent can readily rotate to one side of the backbone or the other, which may lead to improved solid-state packing.

Table 2. Theoretical Energy Values (eV) for DPP−DINI and TPD−DINI Oligomers

polymer	n	HOMO	LUMO	optical LUMO	E_g^{opt}
DPP−DINI	1	−4.93	−2.72	−2.90	2.03
	2	−4.78	−2.82	−3.01	1.77
	3	−4.75	−2.85	−3.06	1.69
	4	−4.74	−2.86	−3.08	1.66
TPD−DINI	1	−5.05	−2.44	−2.72	2.33
	2	−4.96	−2.54	−2.86	2.10
	3	−4.94	−2.64	−2.93	2.01
	4	−4.93	−2.64	−2.96	1.97

Optical Properties of Polymers. The normalized absorption spectra of the polymers displayed in Figure 2 were measured at rt in solutions of chloroform. As a first observation, polymers with the DPP acceptor are substantially red-shifted relative to those containing the TPD acceptor unit, the λ_{max} by as much as 220 nm (compare **P3** with **P6** in Table 1). This is consistent with theoretically calculated spectra, as shown in Figure 1. Note that the computed spectra are for gas phase structures, so any effects of aggregation or other intermolecular interactions are not taken into account.

dx.doi.org/10.1021/ma301987p | *Macromolecules* 2013, 46, 1350−1360

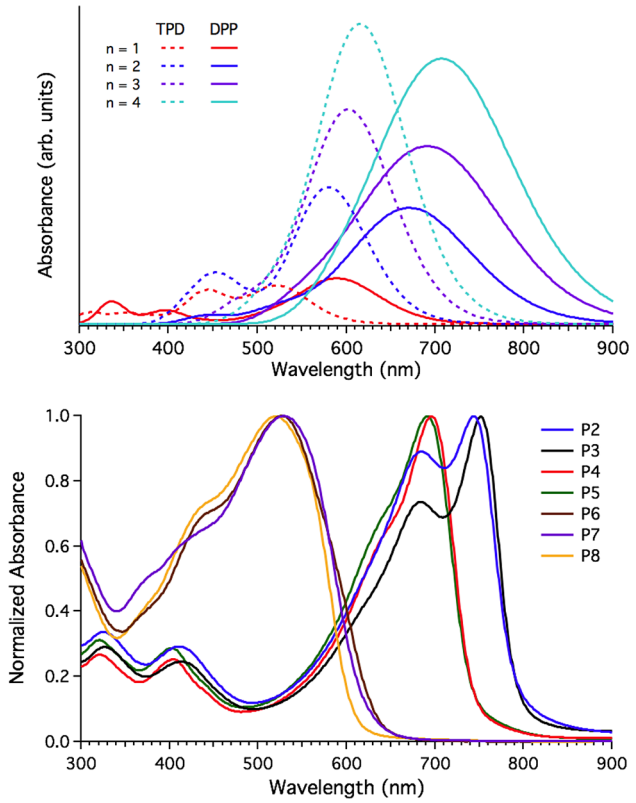

Figure 1. (top) Computed absorption spectra for oligomers of DPP–DINI (solid lines) and TPD–DINI (dashed lines). Spectra were broadened artificially as described in the Experimental Section. (bottom) Normalized absorption spectra of polymers **P2**–**P8** in chloroform solution (**P6** in *o*-dichlorobenzene).

Altering the alkyl chain substitution on the indoloindole unit can dramatically affect the absorption of the polymers. For DPP-containing polymers with structurally analogous 2-ethylhexyl and 2-hexyldecyl substitution on the DINI unit (**P2** and **P3**, respectively), values of λ_{max} are similar, as are values of $\lambda_{0.1max}$. Additionally, the spectra for these two polymers each display a second local maxima at 684 nm. However, the λ_{max} and $\lambda_{0.1max}$ of polymer **P4**, with 9-heptadecanyl substitution, is blue-shifted by ∼50 nm and only displays one maximum at 696 nm. **P5**, also with 9-heptadecanyl substitution on DINI but with a linear *n*-octyl instead of a branched 2-ethylhexyl chain on the DPP unit, displays a similar ∼50 nm blue-shift.

The dramatic difference in the solution absorption spectra of these polymers might be attributed to the relative propensity of the polymers to aggregate in solution.[11] While our gas phase calculations predict virtually no difference in the absorption spectra for these different polymers, three-dimensional modeling (Figure 2) does suggest that steric hindrance in the 9-heptadecanyl chain of **P4** and **P5** with hydrogen atoms in the DINI unit should force the alkyl chains out of plane with the rigid aromatic backbone. However, when the alkyl chain branching occurs in the 2-position, as in **P2** and **P3**, the alkyl chains can more easily rotate to one side of the backbone or the other, which could ultimately allow better molecular packing in the solid state and more pronounced aggregation in solution. Indeed, when solutions of **P2** and **P3** are diluted by a factor of 10 and then 100, the relative intensity of the local maximum around 750 nm as compared to the one at 684 nm systematically decreases, an observation consistent with aggregation being the origin of the observed red-shift. The same trend is observed for the TPD containing polymers, although the relative shifts are much less pronounced and only one maximum is observed for all three polymers.

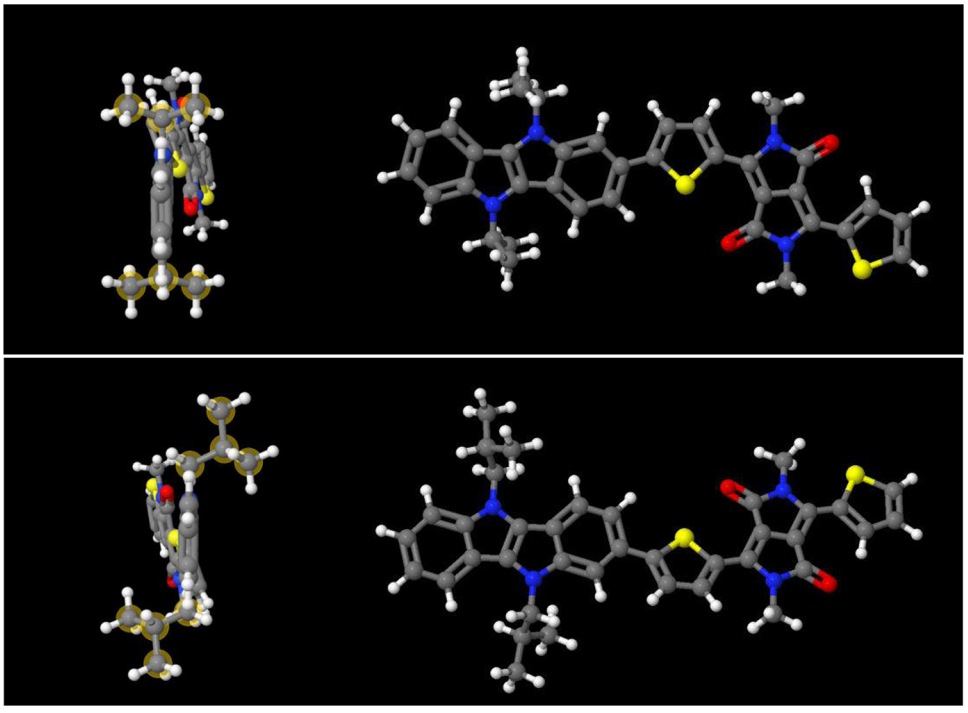

Figure 2. Molecular image representing the lowest energy geometry of a DPP–DINI monomer where the alkyl chain branching occurs in the 1-position (top), as in **P4** and **P5**, and in the 2-position (bottom), as in **P2** and **P3**. The carbon atoms associated with the alkyl chains in the images on the left are highlighted for clarity.

dx.doi.org/10.1021/ma301987p | *Macromolecules* 2013, 46, 1350–1360

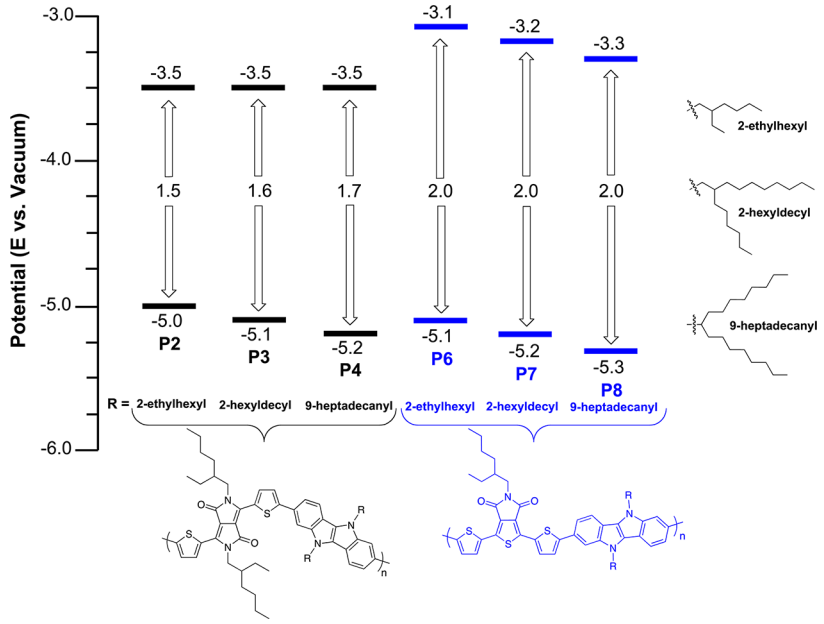

Figure 3. Optical band gaps and energy levels determined for DPP–DINI and TPD–DINI polymers from solution measurements of $\lambda_{0.1max}$ and electrochemical estimates of HOMO values.

The λ_{max} values of the film absorbance spectra of the polymers only red-shift ~10 nm relative to the respective solution spectra (see Figure S2). Interestingly, polymer **P7** develops a shoulder in its solid state absorbance spectrum, which is incidentally consistent with it ability to more easily pack than **P8**.

Electrochemical Characterization of Polymers. Cyclic voltammetry was utilized to evaluate the HOMO energy levels of polymers **P2**–**P8**. A full summary of the data is reported in Table S1 and Figures S3–S10 and includes peak potentials of the oxidation and reduction waves, the ratio of reverse to forward peak current, and $E_{1/2}$ values. Peak-to-peak separations varied between 135 and 190 meV, and the ratio of reverse to forward current varied between 0.16 and 0.77. E_{HOMO} was estimated from $E_{1/2}$ values measured vs Ag/Ag^+ and calibrated against the ferrocene/ferrocenium couple (Fc/Fc^+ measured as 0.09 V vs Ag/Ag^+). The Fc/Fc^+ energy level used in HOMO calculations was assumed to be −4.80 eV.[34] Thus, $E_{HOMO} = -(E_{1/2} + 4.71)$ eV, where $E_{1/2}$ is reported vs Ag/Ag^+. Polymer films were drop cast onto a platinum electrode from solutions with uniform concentrations (1 mg/mL), as it is shown in Figure S10 that higher concentrations (10 mg/mL) could give erroneous results.

A few interesting observations can be made about these voltammograms. The measured HOMO values for these DPP polymers are quite dependent on the alkyl group substitution at the DINI unit. In polymers **P2**, **P3**, and **P4**, with 2-ethylhexyl, 2-hexyldecyl, and 9-heptadecanyl substitution, respectively, the HOMO values are measured as −5.0, −5.1, and −5.2 eV. This is consistent with the trend observed in the open-circuit voltages of devices, with values of V_{OC} measured as 562, 605, and 680 mV for **P2**, **P3**, and **P4**, respectively. When the alkyl chain on the DPP unit is changed from a branched 2-ethylhexyl to a linear *n*-octyl chain (compare results for **P4** and **P5**), no difference is observed in the measured HOMO values.

The same trend in HOMO values with alkyl group substitution is seen in TPD polymers **P6**, **P7**, and **P8**, with HOMO values of −5.1, −5.2, and −5.3 eV, corresponding with 2-ethylhexyl, 2-hexyldecyl, and 9-heptadecanyl substitution. While **P6** was sufficiently soluble in hot dichlorobenzene to make a rough film for a voltammogram, no devices were made for this polymer. However, V_{OC} values in devices of **P7** and **P8** were measured as 757 and 797 mV, consistent with the relative HOMO values of the two polymers, as well as the trend observed for the DPP polymers. Figure 3 illustrates the experimental energy levels for the seven polymers determined from electrochemical film measurements of HOMO values combined with optical gaps determined from $\lambda_{0.1max}$.

Time-Resolved Microwave Conductivity Analysis. To determine the effect of polymer structure on the photophysical properties of bulk heterojunctions of our polymers with $PC_{61}BM$, we carried out time-resolved microwave conductivity (TRMC) measurements on films deposited onto quartz substrates under the same conditions as the devices reported in the Experimental Section. The purpose of these measurements is to evaluate the free carrier generation and decay dynamics in a blend film and correlate it to the microstructure of the bulk heterojunction.

The comparison between films of **P3**:$PC_{61}BM$ and **P4**:$PCB_{61}M$ is shown in Figure 4, where the product of the yield for free carrier generation with the sum of mobilities of electron and holes (eq 2) is plotted against the photon flux of the excitation pulse absorbed by the sample (see Experimental Section for details). The decrease of $\varphi\sum\mu$ with increasing absorbed photon flux has been attributed to non linear exciton–carrier interactions at high light intensities.[16,17] We use eq 3 (Experimental Section) to fit the intensity dependence of $\varphi\sum\mu$ and extrapolate to the low intensity range where $\varphi\sum\mu$ does not depend on light intensity (the linear response regime). Figure 4 shows that the low-intensity limit of $\varphi\sum\mu$ for the **P3**:PCBM sample is an order of magnitude higher than that of **P4**:$PC_{61}BM$. We attribute this to aggregation of the polymer chains in the case of **P3**, as discussed above, that is expected to improve delocalization of charge that has been proposed to enhance free carrier generation.[35−37] On the contrary, the steric interactions of the side chain and the backbone of **P4** cause

dx.doi.org/10.1021/ma301987p | *Macromolecules* 2013, 46, 1350–1360

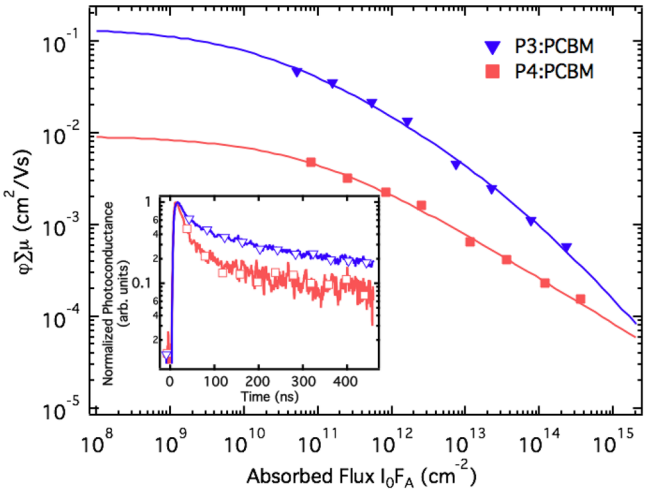

Figure 4. The product of the yield for free carrier generation and the sum of the mobilities of electrons and holes versus absorbed photon flux for blends of **P3**:$PC_{61}BM$ and **P4**:$PC_{61}BM$, measured by TRMC. The solid lines represent fits to the data using eq 3 (see Experimental Section). The inset shows normalized photoconductance transients at an absorbed photon flux of 7×10^{12} photons/(cm^2 pulse).

them to twist out of the plane of the backbone limiting aggregation and causing the blue-shift of the absorption spectrum discussed earlier. We propose that this same structural feature limits the efficiency of free carrier generation in **P4**:$PC_{61}BM$, as the polymer chains are pushed further apart in this case, and delocalization of the hole is limited. The decay times of the photoconductance transients shown in the inset of Figure 4 also show a slightly longer decay for **P3**:$PC_{61}BM$, consistent with previous work on the dependence of photocarrier lifetimes on aggregation.[35,37] We note, however, that unlike these previous systems, no ordering is observed in films of **P3** and **P4** as no diffraction of X-rays was observed from these films (data not shown) despite the prediction of a planar backbone by DFT calculations. Finally, as shown in Figure 4, the LUMO energies of **P3** and **P4** are very similar; therefore, a change in charge generation yield (φ) due to changes in the driving force for free carrier generation can be ignored.

The TRMC results of Figure 4 provide some insight into the improved performance of devices of **P3**:PC61BM. TRMC probes the primary step in photocurrent generation in an OPV device, namely the creation (under very low electric field) of free carriers following photoexitation of the bulk heterojunction. While we cannot exclude differences in $\sum\mu$ of the two samples, the similarity of the two systems (same conjugated system, same $PC_{61}BM$ loading) indicate comparable contribution of the electron mobility to $\sum\mu$. We therefore propose that free carrier generation in **P3**:$PC_{61}BM$ is more efficient due to the proximity of polymer chains in this system, giving the higher J_{sc} observed in OPV devices (see below).

Photovoltaic Characteristics. To investigate and compare photovoltaic properties of the new absorbers, BHJ devices with a configuration of ITO/PEDOT:PSS/polymer:$PC_{61}BM$/Ca/Al were fabricated. Figure 5 shows $J-V$ curves of the devices under illumination with simulated AM1.5 at 100 mW/cm^2. The photovoltaic parameters are summarized in Table 3. The active layer blends for all copolymers investigated were spin-coated from either chloroform or chlorobenzene (CB) solutions depending on solubility. The weight ratios of the polymer/$PC_{61}BM$ in the active layer were also optimized for all polymer

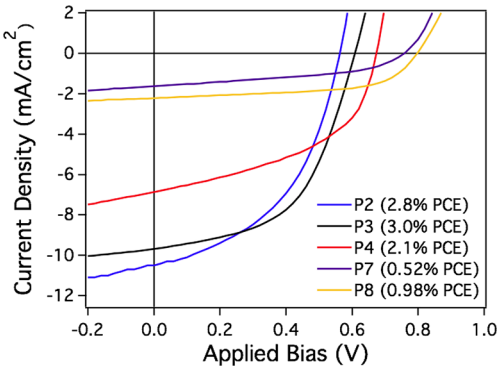

Figure 5. $J-V$ curves of polymer:$PC_{61}BM$ solar cell devices.

Table 3. Device Characteristics of Photovoltaic Solar Cells Based on Polymers P2–P8 with $PC_{61}BM$

polymer	solvent	D:A ratio	V_{OC} (mV)	J_{SC} (mA/cm²)	FF (%)	PCE[d] (%)
P2	$CHCl_3$[a]	1:1	568	10.5	47	2.8
P3	CB[b]	1:2	608	9.7	53	3.0
P4	CB	1:2	673	6.8	48	2.1
P7	CB[c]	1:2	757	1.6	44	0.52
P8	CB[c]	1:2	797	2.2	59	0.98

[a]Chloroform with 1% v/v diiodooctane. [b]Chlorobenzene solution with 10% v/v diiodooctane. [c]Chlorobenzene solutions with 4% v/v diiodoocatne. [d]Approximate PCE.

samples. Comparison of TPD- and DPP-based devices fabricated under comparable processing conditions demonstrates that devices containing TPD-based copolymers generate noticeably higher V_{OC} than those based on the DPP acceptor unit. This observation is consistent with theoretical calculations that predict the HOMO of the $n = 4$ oligomer of TPD-DINI to be 190 meV deeper than that of DPP-DINI. However, despite their higher V_{OC}, devices of **P7** and **P8** suffered from reduced J_{SC}, FF, and PCE relative to those of **P2**–**P4**. The decreased performance of **P7** and **P8** devices might be partially attributed to the hypsochromic shift of the absorption spectra and consequently reduced photon harvest.

Devices of DPP-based polymers, **P2** and **P3**, which contain a primary alkyl substituent on the DINI unit, produced noticeably higher PCE and J_{SC} than that of **P4**. The decreased performance in devices of **P4** might be attributed to the steric interactions between the secondary alkyl chain on the nitrogen atom and the aromatic backbone, as discussed earlier.

■ CONCLUSIONS

In summary, we have designed and synthesized a series of conjugated copolymers comprised of a new electron-rich DINI comonomer moiety and electron-deficeint DPP or TPD moieties, from which BHJ solar cells could be fabricated with relatively efficient preliminary device performance. A significant effect of the size and shape of the pendant alkyl substituents attached to the DINI unit was observed on the optical and electronic properties of the copolymers. Theoretical calculations suggested that branching from the 2-position of the alkyl substituent on DINI (as opposed to the 1-position) should allow for better interchain interactions. These predictions were consistent with the red-shifted absorbance, the higher peak photoconductance, slower photoconductance decay (as determined by time-resolved microwave conductivity), and better

dx.doi.org/10.1021/ma301987p | Macromolecules 2013, 46, 1350–1360

overall device performance observed for polymers with 2-hexyldecyl substituents. The results provide future guidance for the appropriate selection of polymer side chains in OPV device fabrication.

■ ASSOCIATED CONTENT

Supporting Information

Cyclic voltammograms for all polymers, absorption spectra of polymers, geometric structures of some polymers, and ^{1}H NMR spectra for comonomers and copolymers. This material is available free of charge via the Internet at http://pubs.acs.org.

■ AUTHOR INFORMATION

Corresponding Author

*E-mail: Zbyslaw.Owczarczyk@nrel.gov.

Notes

The authors declare no competing financial interest.

■ ACKNOWLEDGMENTS

This work was supported by the U.S. Department of Energy under Contract DE-AC36-08-GO28308 with the National Renewable Energy Laboratory through the DOE SETP program.

■ REFERENCES

(1) Gunes, S.; Neugebauer, H.; Sariciftci, N. S. *Chem. Rev.* **2007**, *107* (4), 1324−1338.

(2) Thompson, B. C.; Frechet, J. M. J. *Angew. Chem., Int. Ed.* **2008**, *47* (1), 58−77.

(3) Cheng, Y. J.; Yang, S. H.; Hsu, C. S. *Chem. Rev.* **2009**, *109* (11), 5868−5923.

(4) Bundgaard, E.; Krebs, F. C. *Sol. Energy Mater. Sol. Cells* **2007**, *91* (11), 954−985.

(5) Beaujuge, P. M.; Frechet, J. M. J. *J. Am. Chem. Soc.* **2010**, *132*, 7595−7579.

(6) Mayer, A. C.; et al. *Adv. Funct. Mater.* **2009**, *19*, 1173−1179.

(7) Dennler, G.; Scharber, M. C.; Brabec, C. J. *Adv. Mater.* **2009**, *21* (13), 1323−1338.

(8) Brabec, C. J.; Cravino, A.; Meissner, D.; Sariciftci, N. S.; Fromherz, T.; Rispens, M. T.; Sanchez, L.; Hummelen, J. C. *Adv. Funct. Mater.* **2001**, *11*, 374−380.

(9) Scharber, M. C.; Mühlbacher, D.; Koppe, M.; Denk, P.; Waldauf, C.; Heeger, A. J.; Brabec, C. J. *Adv. Mater.* **2006**, *18*, 789−794.

(10) Liang, Y.; Xu, Z.; Xia, J.; Tsai, S.; Wu, Y.; Li, Y.; Ray, C.; Yu, L. *Adv. Mater.* **2010**, *22*, 1−4.

(11) Rycel, L. U.; Samuel, C. P.; You, W. *Macromol. Rapid Commun.* **2012**, *33*, 1162−1177.

(12) Zhang, Y.; Zou, J.; Cheuh, C.; Yip, H.; Jen, A. K. *Macromolecules* **2012**, *45*, 5427−5435.

(13) (a) Walker, B.; Tamayo, A. B.; Dang, X.-D.; Zalar, P.; Seo, J. H.; Garcia, A.; Tantiwiwat, M.; Nguyen, T.-Q. *Adv. Funct. Mater.* **2009**, *19*, 3063−3069. (b) Ashraf, R. S.; Chen, Z.; Leem, D. S.; Bronstein, H.; Zhang, W.; Schroeder, B.; Geerts, Y.; Smith, J.; Watkins, S.; Anthopoulos, T. D.; Sirringhaus, H.; de Mello, J. C.; Heeney, M.; McCulloch, I. *Chem. Mater.* **2011**, *23*, 768−770.

(14) (a) Zou, Y. P.; Najari, A.; Berrouard, P.; Beaupre, S.; Aich, B. R.; Tao, Y.; Leclerc, M. *J. Am. Chem. Soc.* **2010**, *132* (15), 5330−5331. (b) Zhang, Y.; Hau, S. K.; Yip, H. L.; Sun, Y.; Acton, O.; Jen, A. K. Y. *Chem. Mater.* **2010**, *22*, 2696−2698. (c) Piliego, C.; Holcombe, T. W.; Douglas, J. D.; Woo, C. H.; Beaujuge, P. M.; Frechet, J. M. J. *J. Am. Chem. Soc.* **2010**, *132*, 7595−7579.

(15) Kroeze, J. E.; Savenije, T. J.; Vermeulen, M. J. W.; Warman, J. M. *J. Phys. Chem. B* **2003**, *107*, 7696−7705.

(16) Ferguson, A. J.; Kopidakis, N.; Shaheen, S. E.; Rumbles, G. *J. Phys. Chem. C* **2011**, *115* (46), 23134−23148.

(17) Dicker, G.; De Haas, M.; Siebbeles, L.; Warman, J. *Phys. Rev. B* **2004**, *70*, 1−8.

(18) Frisch, M. J.; Trucks, G. W.; Schlegel, H. B.; Scuseria, G. E.; Robb, M. A.; Cheeseman, J. R.; Scalmani, G.; Barone, V.; Mennucci, B.; Petersson, G. A.; Nakatsuji, H.; Caricato, M.; Li, X.; Hratchian, H. P.; Izmaylov, A. F.; Bloino, J.; Zheng, G.; Sonnenberg, J. L.; Hada, M.; Ehara, M.; Toyota, K.; Fukuda, R.; Hasegawa, J.; Ishida, M.; Nakajima, T.; Honda, Y.; Kitao, O.; Nakai, H.; Vreven, T.; Montgomery, J. A., Jr.; Peralta, J. E.; Ogliaro, F.; Bearpark, M.; Heyd, J. J.; Brothers, E.; Kudin, K. N.; Staroverov, V. N.; Keith, T.; Kobayashi, R.; Normand, J.; Raghavachari, K.; Rendell, A.; Burant, J. C.; Iyengar, S. S.; Tomasi, J.; Cossi, M.; Rega, N.; Millam, J. M.; Klene, M.; Knox, J. E.; Cross, J. B.; Bakken, V.; Adamo, C.; Jaramillo, J.; Gomperts, R.; Stratmann, R. E.; Yazyev, O.; Austin, A. J.; Cammi, R.; Pomelli, C.; Ochterski, J. W.; Martin, R. L.; Morokuma, K.; Zakrzewski, V.; Voth, G. A.; Salvador, P.; Dannenberg, J. J.; Dapprich, S.; Daniels, A. D.; Farkas, O. G.; Foresman, J. B.; Ortiz, J. V.; Cioslowski, J.; Fox, D. J. Gaussian, Inc., Wallingford, CT, 2010.

(19) http://www.jmol.org/.

(20) Klieg, A.; Haas, K. *Chem. Ber.* **1911**, *44*, 1209.

(21) Ruggli, P. *Chem. Ber.* **1917**, *50*, 883.

(22) Jin, Y.; Ju, J.; Kim, K.; Lee, S.; Song, S.; Kim, J.; Park, S. H.; Lee, K.; Suh, H. *Bull. Korean Chem. Soc.* **2006**, *27* (7), 1043−1047.

(23) Barrscheres, L. H.; Li, L. A. *Can. J. Chem.* **1983**, *61*, 1784−1792.

(24) (a) Grosu, I.; Ple, G.; Mager, S.; Mesaros, E.; Dulau, A.; Gego, C. *Tetrahedron* **1998**, *54*, 2905. (b) Cammidge, A. N.; Crepy, K. V. L *J. Org. Chem.* **2003**, *68*, 6832−6835. (c) Clayden, J. *Tetrahedron* **2004**, *60*, 4335−4436.

(25) Blouin, N.; Michaud, A.; Gendron, D.; Wakim, S.; Blair, E.; Plesu, R. N.; Bellette, M.; Durocher, G.; Tao, Y.; Leclerc, M. *J. Am. Chem. Soc.* **2008**, *130* (2), 732−742.

(26) Najari, A.; Beaupre, S.; Berrouard, P.; Zou, Y. P.; Pouliot, J. R.; Lepage-Perusse, C.; Leclerc, M. *Adv. Funct. Mater.* **2011**, *21* (4), 718−728.

(27) Zhou, M.; Huang, J.; Guan, R. Chinese Patent 102344550 A, 2012.

(28) Nielsen, K. T.; Bechgaard, K.; Krebs, F. C. *Macromolecules* **2005**, *38* (3), 658−659.

(29) Murry, M. M.; Kaszynski, P.; Kaisaki, D. A.; Chang, W.; Dougherty, D. A. *J. Am. Chem. Soc.* **1994**, *116*, 8152−8161.

(30) Hartwig, J. F.; Carrow, B. P. *J. Am. Chem. Soc.* **2011**, *133*, 2116−2119.

(31) Park, J. K.; Jo, J.; Seo, J. H.; Moon, J. S.; Park, Y. D.; Lee, K.; Heeger, A. J.; Bazan, G. C. *Adv. Mater.* **2011**, *23*, 2430−2435.

(32) (a) Szarko, J. M.; et al. *Adv. Mater.* **2010**, *22*, 5468−5472. (b) Biniek, L. *Macromolecules* **2010**, *43*, 9779−9786.

(33) Piliego, C.; Holcombe, T. W.; Douglas, J. D.; Woo, C. H.; Beaujuge, P. M.; Frechet, J. M. J. *J. Am. Chem. Soc.* **2010**, *132* (22), 7595−7596.

(34) Pommerehne, J.; Vestweber, H.; Guss, W.; Mahrt, R. F.; Bassler, H.; Porsch, M.; Daub, J. *Adv. Mater.* **1995**, *7* (6), 551−554.

(35) Rance, W. L.; Rupert, B. L.; Mitchell, W. J.; Kose, M. E.; Ginley, D. S.; Shaheen, S. E.; Rumbles, G.; Kopidakis, N. *J. Phys. Chem. C* **2010**, *114*, 22269−22276.

(36) Murthy, D. H. K.; Gao, M.; Vermeulen, M. J. W.; Siebbeles, L. D. A.; Savenije, T. J. *J. Phys. Chem. C* **2012**, *116*, 9214−9220.

(37) Braunecker, W. A.; Owczarczyk, Z. R.; Garcia, A.; Kopidakis, N.; Larsen, R. E.; Hammond, S. R.; Ginley, D. S.; Olson, D. C. *Chem. Mater.* **2012**, *24*, 1346−1356.